



HAL
open science

Structure, Rheological Behavior, and in Situ Local Flow Fields of Cellulose Nanocrystal Dispersions during Cross-Flow Ultrafiltration

Candice Rey, Nicolas Hengl, Stéphane Baup, Mohamed Karrouch, Erwan Gicquel, Alain Dufresne, Henda Djeridi, Rajeev Dattani, Yong Jin, Frédéric Pignon

► **To cite this version:**

Candice Rey, Nicolas Hengl, Stéphane Baup, Mohamed Karrouch, Erwan Gicquel, et al.. Structure, Rheological Behavior, and in Situ Local Flow Fields of Cellulose Nanocrystal Dispersions during Cross-Flow Ultrafiltration. ACS Sustainable Chemistry & Engineering, 2019, 7 (12), pp.10679-10689. 10.1021/acssuschemeng.9b01333 . hal-02159402

HAL Id: hal-02159402

<https://hal.science/hal-02159402v1>

Submitted on 29 Aug 2022

HAL is a multi-disciplinary open access archive for the deposit and dissemination of scientific research documents, whether they are published or not. The documents may come from teaching and research institutions in France or abroad, or from public or private research centers.

L'archive ouverte pluridisciplinaire **HAL**, est destinée au dépôt et à la diffusion de documents scientifiques de niveau recherche, publiés ou non, émanant des établissements d'enseignement et de recherche français ou étrangers, des laboratoires publics ou privés.

Structure, Rheological Behavior and *in-situ* Local Flow Fields of Cellulose Nanocrystal Dispersions During Cross-flow Ultrafiltration.

C. Rey,^{†,‡} N. Hengl,^{†}, S. Baup,[†] M. Karrouch,[†] E. Gicquel,[‡] A. Dufresne,[‡] H. Djeridi,[§] R. Dattani,[¶] Y. Jin,^ζ F. Pignon,^{†*}*

[†]Univ. Grenoble Alpes, CNRS, Grenoble INP*, LRP, 38000 Grenoble, France

[‡]Univ. Grenoble Alpes, CNRS, Grenoble INP*, LGP2, 38000 Grenoble, France

[§]Univ. Grenoble Alpes, CNRS, Grenoble INP*, LEGI, 38000 Grenoble, France

(* Institute of Engineering Univ. Grenoble Alpes)

[¶]ESRF, The European Synchrotron, CS 40220, 38043 Grenoble Cedex 9, France

^ζSichuan University , College of Light Industry, Textile & Food Engineering, No.24 South Section 1, Yihuan Road, Chengdu, Sichuan, CN 610041

Corresponding Authors

*E-mail: frederic.pignon@univ-grenoble-alpes.fr

*E-mail: nicolas.hengl@univ-grenoble-alpes.fr

KEY WORDS: cellulose nanocrystals, cross-flow ultrafiltration, micro-PIV, velocity field, shear stress, concentration polarization layer.

ABSTRACT

This study focuses on investigating the phenomena involved in the formation of the concentration polarization and fouling layer during the cross-flow ultrafiltration process of cellulose nanocrystal (CNC) suspensions. Thanks to new cross-flow ultrafiltration cells specially designed experiments of firstly time resolved *in-situ* Small Angle X-ray Scattering (SAXS) and secondly time resolved in-situ micro Particle Image Velocimetry (micro-PIV) at the vicinity of the membrane surface during filtration were performed. These two methods have given access to the concentration profiles and the velocity field as a function of the distance z from the membrane surface within the concentration polarization layers. The results obtained show an increase in particles concentration related to a decrease in the velocity within the layers formed during the process. This information linked to the rheological behavior of the suspensions permitted to access the calculated stress field within the concentrated layers during the cross-flow ultrafiltration process. Three different areas of shear stress/shear rate behaviors near the membrane surface have been emphasized. The important role of the rheological behavior and inter particle interaction in the dynamic evolution in space and time of the accumulated layers has been highlighted.

INTRODUCTION

Cellulose nanocrystals (CNCs) are an interesting new kind of natural crystals that are very useful in the development of innovative bio-based materials. An exponentially increasing number of works is devoted to understand and control the structural organization of these colloidal systems¹ and the way they are chemically treated and processed, in order to reach specific functional properties in many industrial applications.² We can notice the use of these cellulose nanomaterials for reinforcement applications, barrier properties, iridescence optical properties,

packaging, adhesives, electronic display materials, and optical encryption technologies.^{3,4} Nanocomposites can be processed by casting/evaporation or more conventional techniques such as extrusion, injection molding, compression molding, film casting, electrospinning and spin coating.⁵

However, for such applications challenges are mainly related to affordable up-scaling production routes of CNC. CNC production yield is linked to the ability of the process used to separate the nanocrystals extracted during or after the hydrolysis process. Indeed, the extraction of crystalline cellulosic regions from native cellulose is based on a simple acid hydrolysis process. The actual production yield ranges from 20 to 50 % depending on the cellulose source and hydrolysis conditions.⁴ The use of membrane separation processes like cross-flow ultrafiltration could be an innovative solution to increase the yield of CNC production and potentially help in firstly improve their size homogeneity and secondly reach higher solid content for the produced CNC suspensions. However, the cross-flow ultrafiltration process is limited by the appearance of two phenomena reducing its performance: concentration polarization and fouling of the membrane. Indeed, under the simultaneous action of the shear induced by the flow and the transmembrane pressure (TMP), the particles or solutes accumulate at the membrane surface, thus reducing filtration performance.⁶⁻¹¹

In order to improve the performance of the cross-flow ultrafiltration process in industrial applications an important point is to understand the concentrated phenomenon induced by the cross-flow and transmembrane pressure near the membrane surface. These phenomena are related to *i*) the filtration conditions, *ii*) the rheological and structural properties of the filtered CNC suspension and *iii*) the equation of state of the suspension (osmotic pressure/volume fraction dependence). One way to understand this phenomenon is to bring a better knowledge on

the spatio-temporal evolutions of firstly the nanoparticle accumulation and secondly the hydrodynamic fields within the concentration polarization layers near the membrane surface.

Concerning the concentration accumulation and structural organization of the nanoparticles near the membrane surface, several investigations have probed the deposit formation at different length scales by means of different approaches. Chen et al.¹² proposed a review of *in-situ* monitoring techniques developed. They can be classified according to the length scale probed. Firstly, at the micrometer length scale some optical non-invasive methods have been implemented like optical, confocal or fluorescence microscopy,¹³⁻¹⁵ holographic interferometry,¹⁶ nuclear magnetic resonance (NMR),¹⁷ optical method using a laser sheet¹⁸⁻²⁰ or microfluidic devices associated to direct micrometer optical observation of clogging dynamics in micro-channels.^{21,22} At higher length scale, direct optical observation has been performed during cross-flow filtration²³ and some recent measurements by fluid dynamic gauging have investigated *in-situ* the thickness and cohesive strength of cake fouling layers.²⁴

Secondly, some studies tried to reveal the formation of concentrated layers at nanometer length scale using *in-situ* and *ex-situ* measurements. As an example *in-situ* or *ex-situ* small-angle neutron scattering (SANS) measurements,²⁵⁻²⁷ or a combination of static light scattering (SLS), SANS and local birefringence techniques.²⁸ More recently ultrafiltration cells dedicated to small angle X-ray scattering (SAXS) measurements have been developed in dead-end mode²⁹⁻³¹ or cross-flow mode (coupled or not to ultrasound).³²⁻³⁶ These equipments allowed getting access to the spatial and temporal *in-situ* structural organization and concentration profile evolutions during ultrafiltration of colloidal suspensions.

Jin et al.³⁵ have investigated for the first time, *in-situ* SAXS measurements of concentrated layers of starch and cellulose nanocrystals suspensions during cross-flow ultrafiltration. They revealed

the general trend of accumulation mechanisms of CNC at the membrane surface and the benefit of ultrasound on the mass transfer during the separation process. Some precedent works have allowed to measure or predict the mean velocity field during filtration processes.³⁷⁻³⁹

Nevertheless, to go further in the understanding of the concentration polarization phenomena induced by ultrafiltration, one missing information until now, is the velocity fields inside the accumulated layers and the corresponding development allowing to get access to this important parameter during the filtration process. With this knowledge, the spatio-temporal stability of the process and the related mechanisms, would be easily predicted or controlled.

The objective of this study is to access to the time and spatial evolutions of the concentration, velocity field and calculated shear stress fields inside the accumulated layer during cross-flow ultrafiltration of CNC suspensions. To reach this objective, cross-flow ultrafiltration cells were designed to perform firstly time-resolved *in-situ* SAXS experiments and secondly time-resolved *in-situ* micro particle image velocimetry (micro-PIV) at the vicinity of the membrane surface during filtration.

Firstly, SAXS measurements have allowed deducing the concentration profile evolutions as a function of time and z distance from the membrane surface. In parallel, micro-PIV measurements in exactly the same filtration conditions, have allowed to deduce the velocity profiles as a function of z and time. The correlation of these results with the rheological behavior of the suspensions have permitted to access the calculated stress field within the concentration polarization and fouling layer during ultrafiltration of CNC suspensions. Three different regions near the membrane surface have been highlighted with different shear-stress/shear-rate behaviors. These results contribute to a better understanding of the concentration polarization

phenomena and will offer new opportunities to develop the membrane separation process in the purpose of increasing the yield of CNC production with higher solid content of the suspensions.

MATERIALS AND METHODS

Materials and sample preparation. Cellulose nanocrystals (CNC) were purchased from Umaine Development Center (University of Maine, USA) as a suspension in water with a stock concentration of $C = 12.2$ wt%. Dilute samples at several concentrations were obtained by dilution of the stock suspension with deionized water, followed by 2 hours of vigorous stirring. The CNC particles have a mean size of 10 nm in width and 150 nm in length. The effect of sonication on the rheological and colloidal properties of these CNC suspensions has been studied in details in a dedicated precedent collaborating work.⁴⁰ In the present article, the suspensions studied were non-sonicated in order to keep the initial properties of the purchased system in the aim of their potential usage at an industrial scale.

Phase diagram of the suspensions. Samples from 1 to 12 wt% (with 1 wt% steps) were poured into 5 mL sealed glass vials and allowed to rest for at least 10 days at room temperature. These vials were observed between crossed-polars and pictures were recorded using a digital camera. The isotropic/anisotropic phase ratio was obtained from the height of each phase measured on these images.

Rheometric measurement. Rheometric measurements with a cone - plate geometry of 49 mm in diameter and $4^{\circ}21'$ angle, were performed using a shear rate controlled rheometer (ARG2, TA Instrument) in the same conditions as³⁴. The surface of the plate geometry has been covered with sand paper with a roughness of 200 μm , in order to avoid interfacial effect. Measurements were performed at a fixed temperature of 25 ± 1 °C and evaporation proof system has been added to guarantee the saturation of the atmosphere of the sample.

SAXS cross-flow ultrafiltration cell. A SAXS coupled to cross-flow ultrafiltration cell was designed to measure *in-situ* structural organization and concentration profiles of the colloidal suspensions during filtration time and as a function of the distance z from the membrane surface (Fig. 1a, b). The cell was made of transparent polycarbonate. The membranes used (100 kD, Pleyade, Orelis environnement) are in polyethersulfone. Two polycarbonate pieces composed the filtration cell, with a upper part for the retentate channel and a lower part for the permeate channel. The membrane is strengthened between these two parts of the cell. The retentate channel has a flow section of 7.4 mm z high x 4 mm y x 100 mm long in x cross-flow direction. Three windows positioned at 43 mm of each other, are used for observation at the entrance, the middle and the outlet of the cell. The $z_c = 0$ position of the filtration cell relates to the edge of the membrane in contact with the lower part of the cell. A (Mono pump LF series, Axflow) has been used to pump the feed suspension from a high pressure tank (Millipore). Purified compressed air was applied to the rig and the retentate pressure P was measured with a pressure gauge (FP 110 FGP Sensors & Instrument) at the inlet and outlet of the cell. A flow meter (Optiflux 6300C flow meter, Krohne) was used to measure continuously the cross-flow flux Q . The permeate flux was recovered in a small tank and a balance (Precisa 400 M) allowed to measure the weight during time with an accuracy of 0.001 g every 5 s. A cryo thermostat (Thermo&Scientific SC, 150 A25, HAAKE) was used to fixed and monitor the temperature at 25 °C during the filtration (**Fig. 1c**).

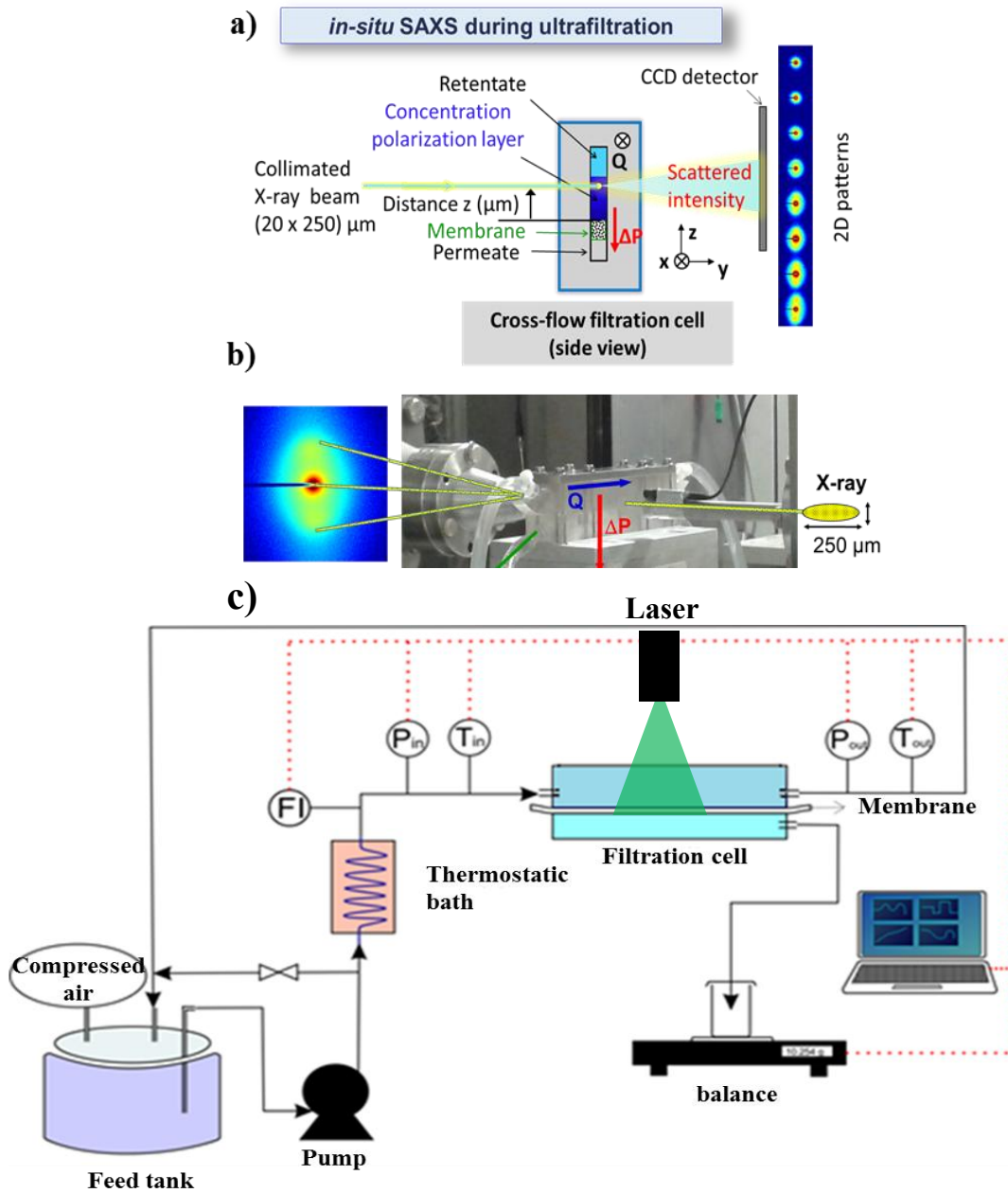


Fig. 1. a) schematic description, b) picture of the *in-situ* SAXS measurements under cross-flow ultrafiltration process and c) overview experimental setup of cross-flow filtration.

CNC suspensions were filtered in several steps (**Fig. 6c**). According to Table 1, only the last filtration step (step 3) will be presented to emphasize concentration polarization or fouling phenomena.

Table1. Different filtration steps and operating conditions for CNC suspensions.

Filtration steps	Flow rate (L.min ⁻¹)	TMP pressure (.10 ⁵ Pa)	Filtration Time (min)
Step 1	0.3	1.1	25
Step 2	0.1	1.1	36
Step 3	0.06	1.1	167

***in-situ* SAXS cross-flow filtration: conditions and analysis.** SAXS experiments were performed at ID02 TRUSAXS beamline⁴¹ of the European Synchrotron Radiation Facility (ESRF, Grenoble, France). The incident X rays beam has a wavelength of $\lambda = 0.1$ nm. To reach a high spatial resolution, the X-ray beam was highly collimated in the vertical and horizontal directions, with a corresponding Full Width at Half Maximum (FWHM) (20 μm (FWHM) vertically and 400 μm (FWHM) horizontally). The sample-to-detector distances were fixed to 2 m and 10 m. The scattering vector q cover the range: $2 \cdot 10^{-2} \text{ nm}^{-1} \leq q \leq 2 \text{ nm}^{-1}$, $q = (4\pi/\lambda)\sin(\theta/2)$ and θ is the scattering angle. The corresponding ($\lambda = 2\pi/q$) length scale range is 3.14 nm $\leq \lambda \leq 314$ nm. Motorized stages were used to move the filtration cell in front of the x-ray beam. A rotational stage was used to align the incident beam parallel with the membrane surface. In order to probe the structure at different vertical position, a vertical translation stage was used to place the filtration cell in front of the beam at a certain z point. The incident beam passed through the sample in the filtration cell and the two-dimensional scattered intensity patterns were recorded on a high-resolution CCD detector (**Fig. 1a,b**).

The analysis of the SAXS patterns registered in the cross-flow cell is the same which has already been described in preceding works.³²⁻³⁴ Four different zones were defined by measuring the transmitted X-ray signal as a function of the distance z_c through the SAXS cross-flow filtration cell. This analysis has allowed to define the minimal distance z_c above which the scattered intensity is not influenced by the scattering of the permeate channel and the membrane.³² This z_c position was fixed at zero ($z_c = 0$). The minimal distance above which the SAXS data are usable was then $z = 50 \mu\text{m}$. Absolute intensity scale of the scattered intensity ($I(q)$) was deduced from azimuthally averaged of the scattering patterns, after applying standard detector corrections and normalization. Before the filtration experiments with CNC suspensions, the cell was filled with demineralized water and the normalized background scattering of the cell was firstly registered. This background scattering of the cell filled with water was systematically subtracted to the scattering of the CNC suspensions for all filtration experiments.³²⁻³⁵

Calibration of volume fraction (or concentration) as a function of interparticle distance. An initial investigation stage of nine different suspensions of known concentrations from 1 wt% to 12.2 wt% was probed by flow through capillary cell with a diameter of 2 mm. This stage allowed establishing the evolution of the scattered intensity as a function of CNC concentration. A Kratky plot (corresponding to $q^2 \cdot I(q)$ vs q) analysis was performed to measure the average interparticular distance (d) between the cellulose nanocrystals (**Fig. 2a**). In this representation, $d = 2\pi/q_{\text{peak}}$, where q_{peak} is the position of the scattered intensity maximum. This analysis allows highlighting wave vector value corresponding to the maximum scattered intensity for each concentration, which is directly linked to the inter-particular distance d by the following law: $d = 2\pi/q_{\text{peak}}$. From this analysis, the interparticle distance was related to the known initial concentration or volume fraction as shown in **Fig. 2b**. The fit exponential of this curve gives

access to the relationship between volume fraction ϕ (or mass concentration C) and the

interparticle distance d : $\phi = \left(\frac{26.433}{1.6}\right) \times e^{(-0.028771 \times d)}$ or $C = 26.433 \times e^{(-0.028771 \times d)}$

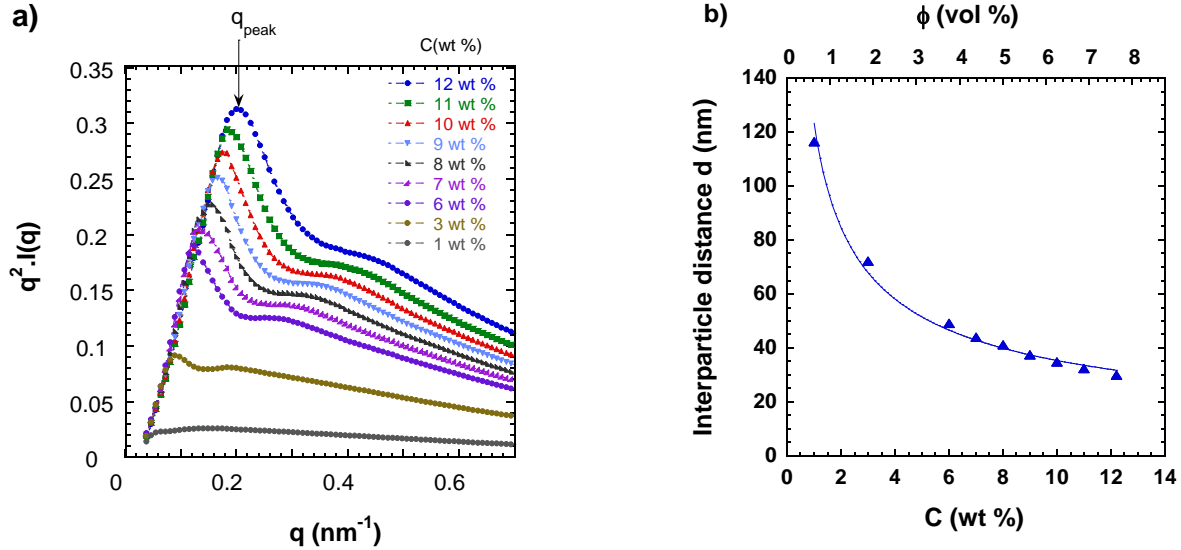


Fig. 2.a) Kratky plot ($q^2 \cdot I(q)$ vs q) of the scattering intensity $I(q)$ at different volume fractions (or mass concentration) of CNC suspensions, b) Interparticle distance as a function of CNC concentration or CNC volume fraction deduced from the Kratky plot analysis.

From this calibration it is then possible to relate the scattered intensity measurement in the filtration cell at a certain distance z_c , to its corresponding q_{peak} , then interparticle distance d and get access to its corresponding volume fraction (or concentration).

***In-situ* micro-PIV: velocity field measurements during cross-flow ultrafiltration process.** A

Plexiglas (PMMA) cross-flow filtration cell was specifically designed to allow a complete visualization of the flow field within the accumulated layers during cross-flow ultrafiltration.

Micro-PIV technique was implemented to measure the velocity field near the membrane surface during the filtration of CNC suspensions. The dimensions of the feed channel were the same as for the cell used for SAXS filtration coupled experiments. The retentate channel was 100 mm

long in x cross-flow flow direction and the flow section was 7.4 mm z high for 4 mm y large. Micro-PIV measurements are accessible all along the length of the channel thanks to the design of the cell (**Fig. 3**). High-resolution camera synchronized with a pulsed laser were used for the Micro-PIV measurements. The laser used was a Nd:YAG pulsed with a wavelength of 532 nm and a power of 50 mJ/pulses (New Wave Solo). Depending on the flow and geometric characteristics, a specific lens was used to produce 1 mm thick laser sheet. These laser sheet has been located in the middle of the channel in the y direction corresponding to the field of view. Although the camera has a resolution of 2657 x 4000 pixels (Hisense 11M) with a cadency of 15 Hz, a visualization area of 2657 x 2000 pixels was used to optimize the storage size of the pictures. In order to inhibit reflection phenomenon near the wall and surface membrane, polystyrene fluorescent particles 5 μm in diameter (microParticleGmbH) with 532 nm absorbance wavelength and 640 nm emission wavelength, were added to the suspension. To avoid an effect of the adding fluorescent particles, on the filtration and rheological behavior, the concentration has been optimized. Special care has been taken to obtain suitable signals detected by the camera allowing reliable correlation functions and velocity measurements.

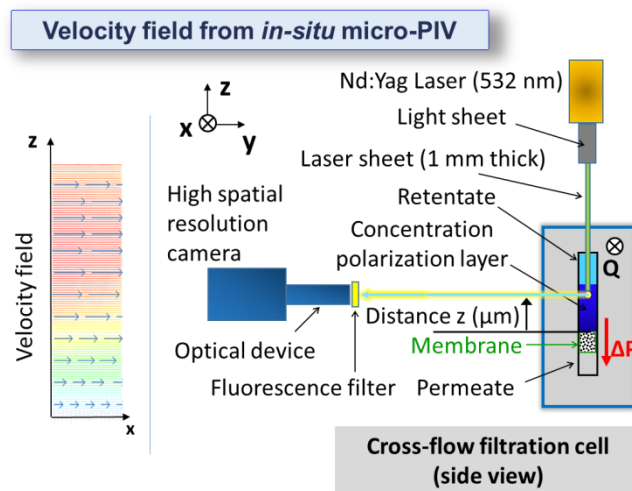


Fig. 3. Scheme of the *in-situ* micro-PIV measurements under cross-flow ultrafiltration process.

The optical device was composed of a Canon 65 mm MPE lens linked to a filter (LaVision) with a range of 545 to 800 nm. During the filtration, 200 pairs of images have been acquired with time laps between two images of 150 μs considering the inlet velocity value of about 0.06 m s^{-1} and a particles displacement of around 8 pixels in region of interest.³⁷ To calculate the velocity field, specific processing based on adaptive cross-correlation between two successive frames, in small sub-domain, has been used. This technique requires a selection of interrogation windows size for the calculation of the velocity especially in regions of high gradients near the wall. The number of image frames allowed a good statistical convergence. A calibration target was used to convert the pixel into physical space. Due to high spatial-resolution of the camera, and the size of interrogation areas, an accurate calculation of the mean velocity components and velocity gradients has been obtained as well as the strain rate tensor each 30 μm of distance above the membrane surface.

RESULTS AND DISCUSSION

Phase diagram of CNC suspensions. CNC suspensions are known to exhibit a phase separation behavior with two coexisting phases, one isotropic phase and one crystalline phase.^{40,42-44} At rest, over time these two phases separate as the crystalline phase has a higher density due to the formation of micro domains orientated along a helicoidally axis, also called a cholesteric (or chiral nematic) organization of the CNC. In recent work⁴⁰ the impact of sonication on the phase diagram and rheological behavior has been studied in details. The results obtained have shown that sonication induce a decrease of the inter-particle distance, a strong decrease of the viscosity and remarkable changes in the liquid crystalline behavior, while sonicated and non-sonicated suspensions were stable over time. These effects can be attributed to a decrease in the aspect ratio of the suspended particles, which varies from a high value before sonication due to

the presence of elongated bundles to a lower value after sonication that promotes individualization. In the present work we have focused on the non-sonicated samples in order to keep the initial properties of the purchased system in the aim of their potential usage at an industrial scale. From the optical observation in cross-polarization, the isotropic/anisotropic phase ratio was deduced from the height of each phase, as shown on **Fig. 4 a,b**. Two critical concentrations were deduced as the linear extrapolation in the biphasic gap at 0 and 100 vol %. The first critical concentration C_i defines the beginning of the biphasic regime $C_i \sim 5.8$ wt% ($\phi_i = 3.63$) and the second critical concentration C_a corresponds to the fully anisotropic phase $C_a \sim 9$ wt % ($\phi_a = 5.62$). Below C_i only isotropic phase is present in the whole part of the sample. Between C_i and C_a , cross-polarized images show the formation of the biphasic phase (in white in pictures) at the bottom of the samples. For increasing concentration in this intermediate domain, the volume fraction of the crystalline phase increases according to the regular increase of the chiral nematic domain. Above C_a , the anisotropic phase represents the whole part of the sample with a gel aspect.

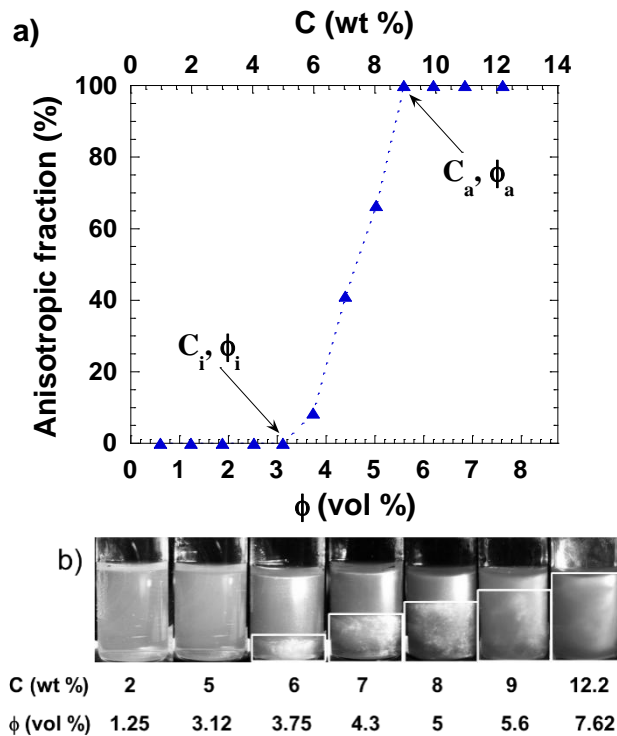


Fig. 4. Phase diagram of CNC suspensions: a) volume fraction of liquid crystalline phase (anisotropic fraction in vol%) as a function of volume fraction (or mass concentration) of CNC suspensions; b) photographs of vials between crossed polars, showing the phase separation of CNC suspensions from 1 to 12 wt%. The lower liquid crystalline phase (anisotropic) is white while the upper isotropic phase appears dark.

Rheometric measurements. The Rheological behavior of the CNC suspensions as a function of the concentration or volume fraction is presented in **Fig. 5a**. Three different regimes have been emphasized corresponding to the three domains highlighted in the phase diagram. For the lower volume fraction below C_i , the suspensions behave as Newtonian fluids. At intermediate concentrations between C_i and C_a a shear thinning behavior is obtained. At the highest concentrations above C_a , CNC suspensions adopt a yield stress fluid behavior. These observations are in agreement with previous rheological measurements on these kinds of CNC suspensions.^{40,42-44}

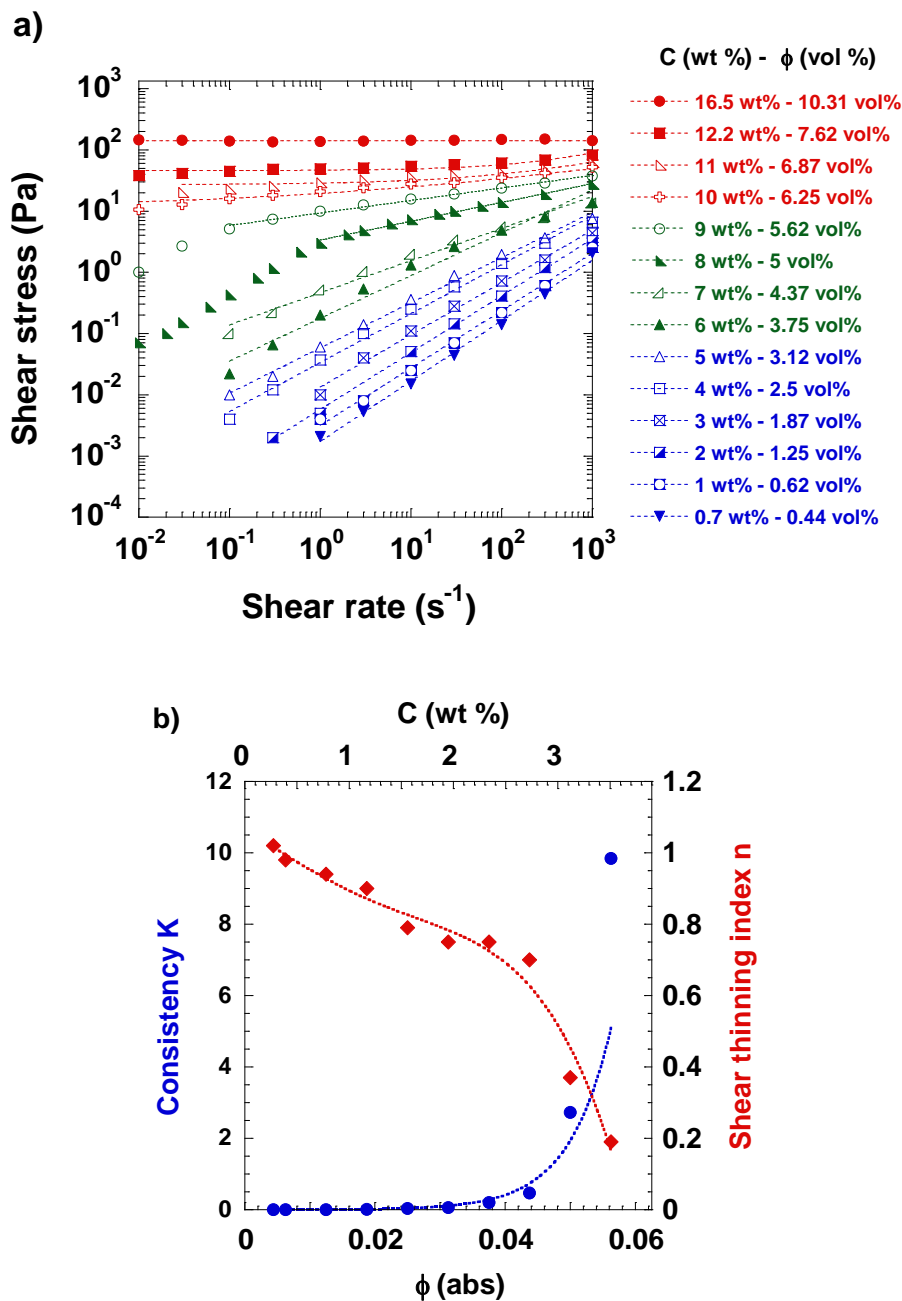


Fig. 5. a) Flow curves (shear stress as a function of the applied shear rate) for CNC suspensions at different weight contents (wt %) and corresponding volume fractions (vol%), obtained in cone and plate rheometric measurements, $T = 25 \pm 1$ °C, dotted lines correspond to linear regression of the experimental data according to power law (Eq. 1) or Herschel-Buckley law (Eq. 2). b)

Consistency K and shear thinning index n as a function of volume fraction ϕ , dotted lines correspond to fitted laws with respectively (Eq. 3) and (Eq. 4).

Method for calculation of the shear stress profile within the accumulated layers during cross-flow ultrafiltration. For the purpose of calculating the stresses reach within the concentrated layers during the cross-flow ultrafiltration process, rheometric flow curves on a wide range of concentrations (relation between shear stress and shear rate), concentration profiles at the membrane surface probed by SAXS and finally micro-PIV measurements (giving access to shear rate in the concentrated layers) were combined as already detailed in our previous work.³² The linear regression of the experimental rheometric data gives power law (Eq. 1) or Herschel-Buckley (Eq. 2) laws depending on the volume fraction or concentration content:

$$\tau(\phi) = K(\phi) \cdot \dot{\gamma}^{n(\phi)} \quad (\text{Eq. 1})$$

$$\tau(\phi) = K(\phi) \cdot \dot{\gamma}^{n(\phi)} + \tau_s(\phi) \quad (\text{Eq. 2})$$

Where ϕ is the concentration in CNC particle (wt%), $\tau(\phi)$ is the shear stress (Pa), $\dot{\gamma}$ the shear rate (s^{-1}), $K(\phi)$ is the consistency, $n(\phi)$ the shear thinning index, and $\tau_s(\phi)$ is the yield stress.

Over the range of CNC concentrations measured during SAXS experiments, any yield stress equation is required. From the fitted laws, the expressions for K and n as function of the concentrations are the following:

$$K(\phi) = 0.00085 \times \exp(154.7 \times \phi) \quad (\text{Eq. 3})$$

$$n(\phi) = -2.29 \cdot 10^5 \times \phi^4 - 14095 \times \phi^3 - 162.75 \times \phi^2 - 10.691 \times \phi + 1.064 \quad (\text{Eq. 4})$$

From the velocity profiles ($V(z)$) obtained by micro-PIV the following expression (Eq. 3) gives access to a calculation of the corresponding shear rate:

$$\dot{\gamma}(z) = \frac{dV}{dz} \quad (\text{Eq. 5})$$

With z the distance from the membrane surface (m), V the velocity measured ($\text{m}\cdot\text{s}^{-1}$).

The expression of the shear stress (Eq. 2) becomes finally:

$$\boldsymbol{\tau}(\phi, \mathbf{z}) = \mathbf{K}(\phi) \cdot \dot{\boldsymbol{\gamma}}(\mathbf{z})^{n(\phi)} + \boldsymbol{\tau}_s(\phi, \mathbf{z}) \quad (\text{Eq. 6})$$

The value of $\boldsymbol{\tau}_s(\phi, \mathbf{z})$ is calculated only above 6.25 vol% volume fraction, when a yield stress is measured in the CNC suspensions.

The shear stress within the concentration polarization (Eq. 6), was then calculate during time and as a function of the distance z from the membrane surface, thanks to the knowledge of *i*) the value of the volume fraction measured by SAXS, *ii*) the value of the calculated shear rate deduced from the micro-PIV (Eq. 5) and *iii*) the rheological laws (ϕ) (Eq. 1 to 4). The only assumption made is that the rheological behavior of concentration polarization and gel layers of suspensions in the cross-flow experiment is considered equivalent to those of bulk suspensions having the same particle concentration. This assumptions is difficult to verify, as the only way to measure directly the stresses in the concentration polarization layer, will be to introduce a specific probe at micrometer length-scale without altering the flow.

***In-situ* Concentration profiles during cross-flow ultrafiltration: SAXS analysis.** The value of concentration reached within the concentrated layers formed during the ultrafiltration process is a required information to correlate with the velocity fields and be able to deduce a calculation of the spatial-temporal evolutions of the stress field near the membrane surface. The access to these crucial parameters of the ultrafiltration process is imperative to improve our knowledge in the mechanisms responsible of performance of this industrial process.

During the SAXS experiments, many interesting conclusions have been established and will be described in this part. An important first observation is that a lowering of the membrane due to the transmembrane pressure applied during the ultrafiltration process has been highlighted.

Indeed, no supporting porous media has been inserted below the membrane. As a consequence a lowering of the membrane in the permeate channel has been observed. As explained in our previous work, this lowering of the membrane, for the same filtration conditions, has been evaluated to 350 μm .³² In order to take into account this lowering of the membrane, the results of SAXS experiments will be presented as a function of the distance z from the membrane surface named z (μm) in the graphs, where $z = z_c + 350 \mu\text{m}$.

Several steps of filtration were probed but only the last one (step 3, at $Q = 0.06 \text{ L}\cdot\text{min}^{-1}$, $\text{TMP} = 1.1 \times 10^5 \text{ Pa}$) will be presented in this article because it specifically highlights the phenomena involved in the formation of concentrated layers.

Fig. 6a shows the concentration profiles for this step 3 of filtration as a function of time. At the beginning of this filtration step 3, the value of the concentration reaches 3.3 wt% ($\phi = 2.1 \text{ vol } \%$) at a distance of 350 μm above the membrane surface and recovers the initial value at a distance of about 500 μm above the membrane (**Fig. 6a**). This information highlights the thickness of the concentrated layer at $t = 0 \text{ min}$ which has been previously constructed during steps 1 and 2 performed successively at two decreasing flow rates of $0.3 \text{ L}\cdot\text{min}^{-1}$ and $0.1 \text{ L}\cdot\text{min}^{-1}$ at the same $\text{TMP} = 1.1 \times 10^5 \text{ Pa}$ (**Table 1**). For increasing filtration times in this step 3, the concentration value increases near 350 μm above the membrane surface, and recovers the initial value of concentration at further distances above the membrane surface, which means that the concentrated layer formed during the filtration process becomes thicker for increasing filtration times. At the end of this step 3, it is interesting to notice that between $t = 99 \text{ min}$ and $t = 116 \text{ min}$, the thickness of the concentrated layer is stabilized at 800 μm above the membrane, whereas the concentration value near 350 μm above the membrane increases significantly: 6.4 wt% ($\phi = 4 \text{ vol } \%$) at $t = 99 \text{ min}$, and 8 wt% ($\phi = 5 \text{ vol } \%$) at $t = 116 \text{ min}$. This can be linked to the fact that the

permeate flux stabilizes during this filtration step (11 L.h⁻¹.m⁻² at the beginning of the step 3 and 7 L.h⁻¹.m⁻² since about 40 minutes of filtration) (**Fig. 6c**).

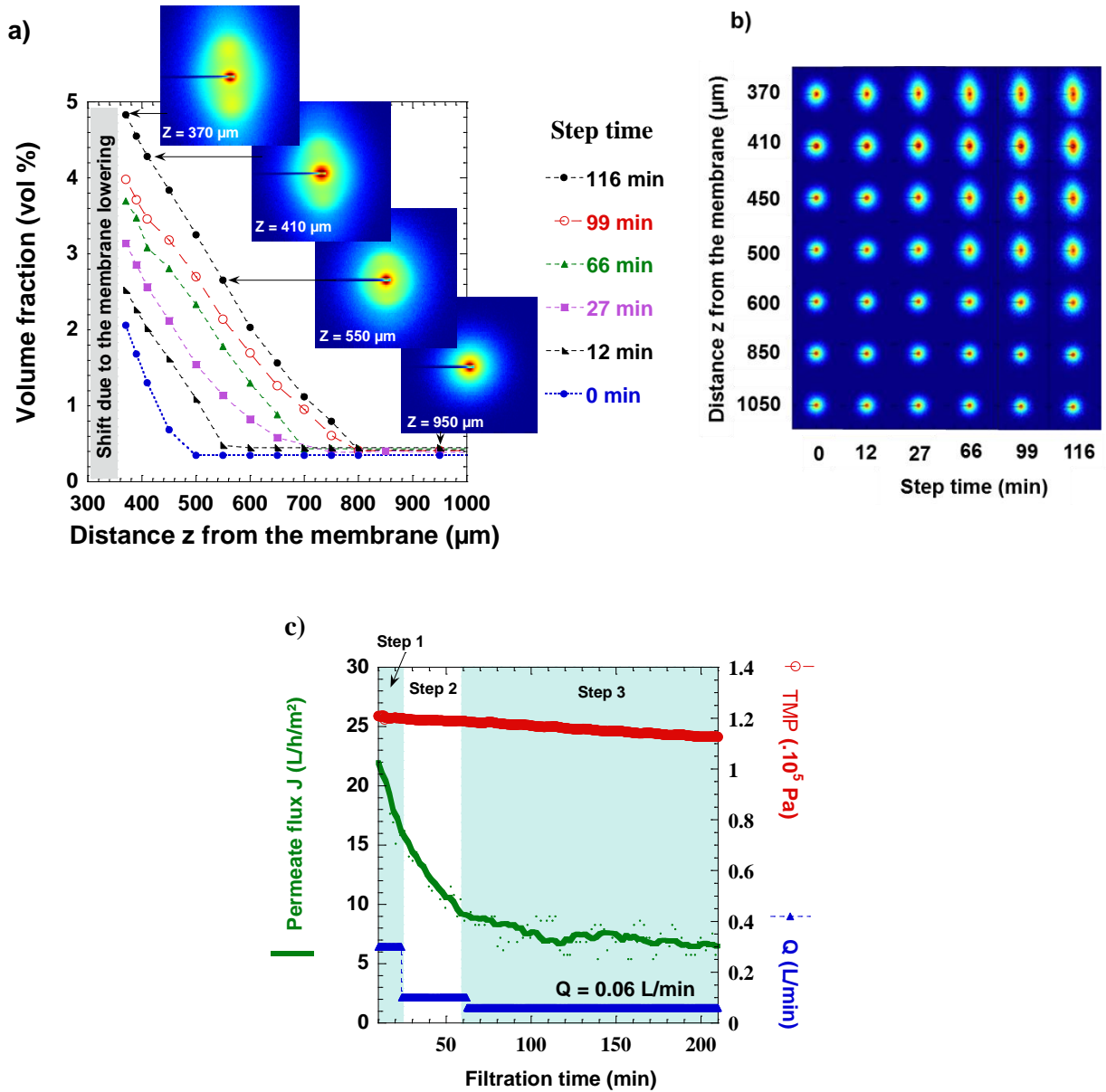


Fig. 6: a) concentration profiles, b) SAXS pattern and c) corresponding permeate flux as a function of filtration conditions for different filtrations steps, obtained during *in-situ* SAXS measurements and during cross-flow ultrafiltration process of CNC suspensions at initial volume fraction 0.437 vol% (0.7 wt%). $Q = 0.06 \text{ L}\cdot\text{min}^{-1}$, $\text{TMP} = 1.1 \times 10^5 \text{ Pa}$, $T = 25 \pm 1 \text{ }^\circ\text{C}$.

The 2D-SAXS patterns (**Fig. 6b**) obtained during these experiments highlight a specific orientation induced by the ultrafiltration process. At the first time of filtration, near 350 μm above the membrane the pattern is slightly anisotropic, which means that CNC shows a specific orientation along the flow direction. These kind of orientation mechanisms under cross-flow ultrafiltration have already been emphasis on others anisotropic colloidal Laponite clay particles suspensions.³² For further distances the 2D-SAXS patterns show an increase in the anisotropy which can be related to an increase in the orientation level of the nanocrystals at the nearest distances from the membrane surface and during their accumulation, under the simultaneous effect of cross-flow and TMP. For increasing filtration times, the SAXS patterns exhibit higher and higher scattering intensity in the vertical direction which is due to the increase in concentration fluctuation in the vertical direction, induced by the regular orientation of CNC with their main axis orientated parallel to the membrane surface. At equilibrium time $t = 116$ min, this specific orientation of CNC extend form $z = 350 \mu\text{m}$ to further distances above the membrane surface until $z = 600 \mu\text{m}$ (**Fig. 6b**).

Velocity field deduced from in-situ micro-PIV. **Fig. 7** shows the velocity profiles as a function of the distance z for increasing time, for the same step 3 of filtration studied by SAXS. At the beginning of this step, the profile at $t = 0$ min exhibits firstly a zero value at $z = 350 \mu\text{m}$ above the membrane surface and then an increase of velocity for further distance above the membrane. Below 350 μm , we can make the conclusion that it exists an area of no flow. This will correspond to the formation of a concentrated layer during the process as emphasis in **Fig. 6a** from SAXS data. For increasing filtration times, the area for which no motion is detected grows continuously. As an example the departure from 0 velocity to the measurement of a first increase in velocity is at $z = 600 \mu\text{m}$ at $t = 44$ min, whereas after 116 min of filtration a first

velocity value is detected at $z = 850 \mu\text{m}$. It is interesting to notice that the velocity profiles exhibit a stabilization of the concentrated layer thickness where no flow is detected, since 99 min of filtration correspond to a stabilization of the permeate flux (**Fig. 6c**).

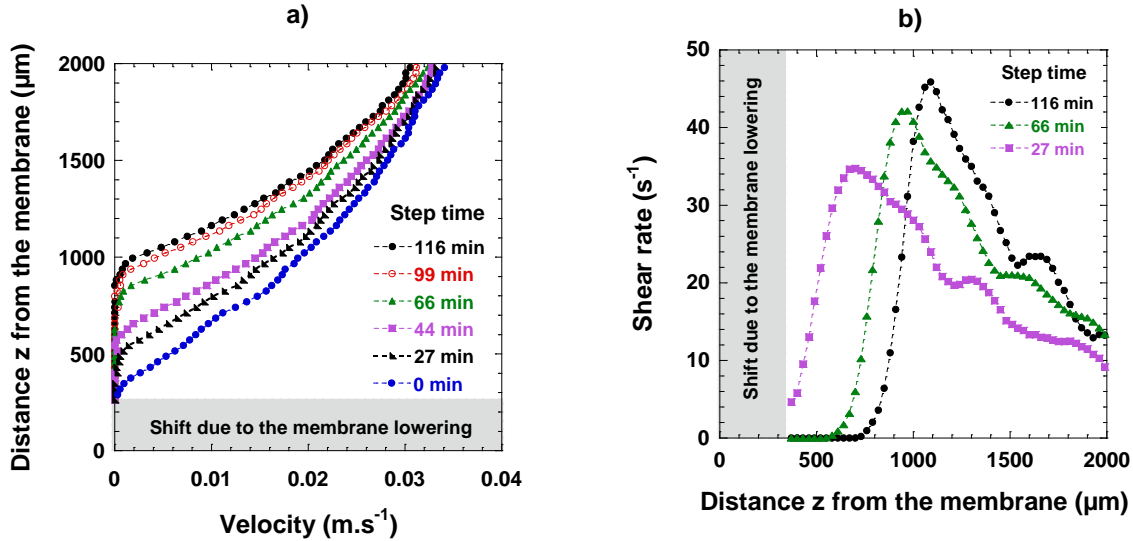


Fig. 7. a) Velocity profiles for CNC suspension as a function of the distance z from the membrane surface (with lowering correction) during cross-flow ultrafiltration obtained by micro-PIV b) corresponding calculated shear rates in the concentrated layer at three different filtration times of step 3. Initial filtered volume fraction 0.437 vol% (0.7 wt %). $Q = 0.06 \text{ L}\cdot\text{min}^{-1}$, $\text{TMP} = 1.1 \times 10^5 \text{ Pa}$, $T = 25 \pm 1 \text{ }^\circ\text{C}$.

The correlation between the concentration profiles obtained by SAXS experiments and the velocity profiles obtained by micro-PIV highlights the existing link between the increase of the concentration within the concentrated layer formed and the reduction of the velocity in this layer, for increasing filtration times.

Shear rate and shear stress in concentrated accumulated layers.

Shear-rate calculated from velocity field. In **Fig. 8** the shear rate profiles calculated from the velocity field measured by micro-PIV (**Fig. 7**) and **Eq. 5**, for several filtration times as a function

of the distance z above the membrane surface is plotted. At $t = 27$ min of filtration, the shear rate is 4.64 s^{-1} near $z = 350 \text{ }\mu\text{m}$ meaning that a flow is involved since this distance z , in good agreement with the PIV result. Then the shear rate profile increases until a maximum value of 35 s^{-1} before decreasing towards the middle of the channel. For increasing filtration times, the shear rate profiles show an increasing thickness of the area for which zero shear rate value is calculated. This area of no -flow extends to $z = 470 \text{ }\mu\text{m}$ at $t = 66$ min and until $z = 620 \text{ }\mu\text{m}$ at $t = 116$ min. For increasing filtration times, the shear rate profiles behave in the same manner as for $t = 27$ min: an increase until 42 s^{-1} and 47 s^{-1} , respectively, for $t = 66$ min and $t = 116$ min, before decreasing. It is interesting to notice that the shear rate profiles start to increase at the same distances z measured for the increase of the velocity profiles (**Fig. 7**). These distances correspond to the layer thickness above which the flow starts to occur.

The shear rate profiles at different filtration times $t = 27$ min, $t = 66$ min and $t = 116$ min exhibit the same three different evolutions as a function of the distance z from the membrane surface, which emphasis a continuous concentrated phenomenon over time. Firstly, close to the membrane surface, the shear rate is equal to zero which corresponds to a region without flow. In this region, CNCs suspensions (around $C = 5 \text{ wt}\%$) behave like a suspension at rest due to the effect of pressure forces. When one moves away from the membrane surface, the shear rate starts to increase to a maximum value. Finally, once this value is reached, it decreases to a minimum value around 20 s^{-1} for a concentration equal to the initial concentration. As observed during the filtration of colloidal suspensions of Laponite³², the thickness of the different zones varies with filtration times, thus modifying the filtration performance.

Shear stress fields calculated within accumulated layers during cross-flow ultrafiltration.

From the already knowledge obtained on the concentration (**Fig. 6**) and shear rate (**Fig. 7**) evolutions as a function of distance z and filtration time on the same system and same procedure, we have the opportunity to calculate the shear stresses inside the accumulated layers. For that purpose we have combined these data (concentration and shear rate), with the rheological laws $\tau(\phi, z)$ (eq. 6) of the CNC suspensions deduced from the rheometric measurements at different volume fractions. One example of this calculation is shown in **Fig. 8** where the volume fraction, calculated shear rate and shear stress are plotted as a function z for three different filtration times. The assumption made is that the rheological behavior of concentration polarization of CNC suspensions in the cross-flow experiment is equivalent to those determined by rheometric measurements in steady state for CNC suspensions having the same volume fraction. The main approximation is that the transient shear stresses in the concentration polarization are calculated from rheological laws deduced from steady state flow curves. This raised the question: is the time dependent evolution of the shear stresses in the concentration polarization layers sufficiently slow to consider that the steady states flow curves of the rheological behavior are relevant to perform the calculations for the range of volume fraction and shear rates involved. In the presented results (**Fig. 8**), in the flowing layers region B or C which would be affected by these time dependent evolutions, the highest volume fraction is 0.03 (abs) corresponding to 3 vol% and the shear rate is lower than 50 s^{-1} . These volume fractions and shear rates domains correspond to a Newtonian behavior of the CNC suspensions for which the transient states duration are of the order of one minute. The kinetic formation of the concentration polarization layers extend on time scales of few tens of minutes as shown on **Fig. 6a** and **Fig. 7a**. Consequently, the steady state flow curves of the rheological behavior of the CNC suspensions

are relevant in first approximation, to calculate the transient state evolutions of the shear stresses in the concentration polarization layers.

At $t = 27$ min of filtration (**Fig. 8a**), we can distinguish two different behavior areas named B and C. The area B corresponds to the increase of the shear rate profile meaning that a flow starts to occur in the polarization concentration layer. This phenomenon is allowed by the decrease of the volume fraction from 3 vol% to the initial volume fraction for the same distances z , until $700 \mu\text{m}$. Over this volume fraction range, it is interesting to note that the rheological behavior of the suspensions is Newtonian (**Fig. 5**) and that the cellulose nanocrystals flow with a random orientation as no anisotropy is detected in the SAXS patterns (**Fig. 6b**). The value of the shear stress imposed by the cross-flow is high enough to involve a flow in the concentrated layer. Since the volume fraction reaches the initial filtered volume fraction value (0.437 vol%) the shear rate decreases meaning that no more concentrated layer influences the flow. This marks the transition to the area C corresponding to the flow where the suspension is circulating in the feed channel out of concentration phenomena. When the filtration time increases to $t = 66$ min (**Fig. 8b**) and $t = 116$ min (**Fig. 8c**), we can observe the appearance of an area named A where the shear rate and shear stress profiles show a zero value until $500 \mu\text{m}$ and $750 \mu\text{m}$ respectively above the membrane. This corresponds to the fouling layer where any flow is measured due to the higher value of the volume fraction. Indeed, in this area A the volume fraction value is higher than 2 vol% and increases until 3.75 vol% at $t = 66$ min and until 4.8 vol% at $t = 116$ min. On these range of volume fraction the rheological behavior is changing from Newtonian to shear thinning, without yield stress. According to rheometric measurements (**Fig. 5a**) a yield stress is reached above 6.25 vol % volume fraction. Consequently in this area the shear stress is calculated with Eq. 6, without taking into account any $\tau_s(\phi, z)$.

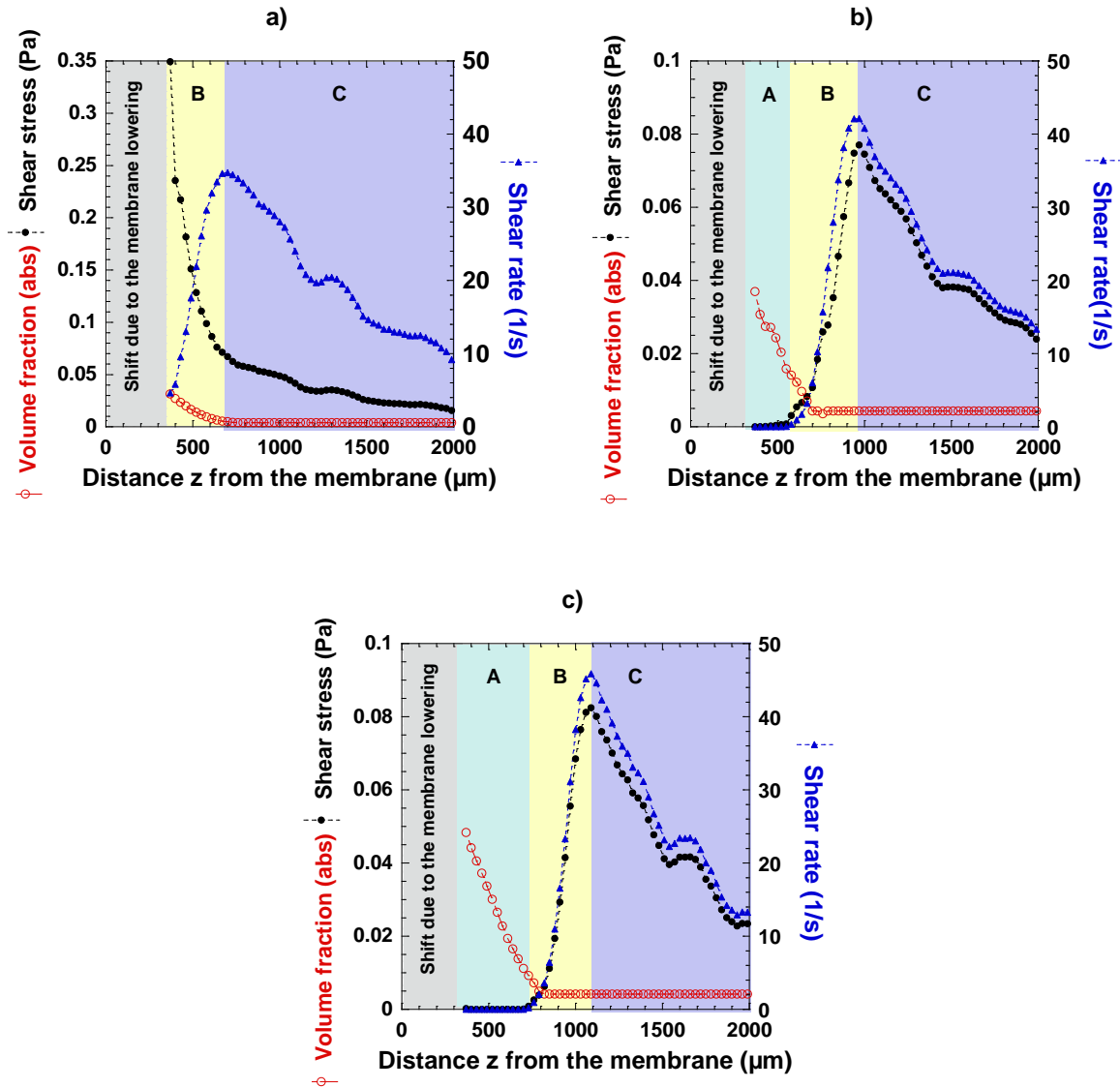


Fig. 8. Behavior regions A, B and C in the concentrated layer formed from CNC suspensions as a function of the distance z from the membrane surface (with the lowering correction) during cross-flow ultrafiltration, for the last step of filtration, step 3, $Q = 0.06 \text{ L}\cdot\text{min}^{-1}$. At filtration time a) $t = 0 \text{ min}$, b) $t = 66 \text{ min}$, c) $t = 116 \text{ min}$. Initial filtered volume fraction $0.437 \text{ vol}\%$ ($0.7 \text{ wt}\%$). $\text{TMP} = 1.1 \times 10^5 \text{ Pa}$, $T = 25 \pm 1 \text{ }^\circ\text{C}$, middle window.

These observations are in good agreement with previous established models which assume that due to a sufficiently high concentration or low shear rates near the membrane surface, the flow

can stop and an arrested layer starts to be formed.^{32,44-46} The shear rate and shear stress profiles increase only since the volume fraction profile reaches values below 2 vol%, corresponding to the transition toward a Newtonian rheological behavior. Thus, the shear stress imposed by the cross-flow is high enough to let the CNC flow. In this region B, corresponding to the concentration polarization layer, the shear forces overcome the colloidal interactions and pressure forces, which allow the initiation of the flow. At higher distances z , the shear rate starts to decrease with the shear stress until reaching the feed channel, this last region is named region C. For increasing filtration times, the same phenomena are observed (**Fig. 8c**). The area A extends on larger z distances z above the membrane surface than for shorter filtration times, in agreement with higher values of volume fraction, in a regime for which the CNC suspension behaves as a shear thinning behavior. The transition from area B to C, at $z = 1100 \mu\text{m}$, is marked by the simultaneous decrease of shear rate and shear stress towards the middle of the cell to join the feed channel.

These concentration phenomena and the existence of different areas A, B and C have been previously observed for others kind of colloidal Laponite clay suspensions.³² It is interesting to notice that for this kind of attractive colloidal system the transitions between areas A and B occurs around the gel to sol transition. That is to say that for Laponite suspensions, the stresses in region A correspond to yield stresses, while in region B the stresses correspond to lower values with a shear thinning behavior of the suspensions. It was thus highlighted that the transitions between these areas A and B are strongly related to the rheological behaviors of the filtered system. For Laponite suspensions, the flow is initiated at the gel to sol transition while for the CNC suspensions the flow is introduced around the transition from shear-thinning to Newtonian behavior. For the CNC suspensions, one possible mechanism inducing this arrested state in area

A, is that the pressure forces imposed by the transmembrane pressure associated to the viscous forces and interparticle interactions, allow maintaining the particles in an arrested state near the membrane surface where the shear forces imposed by the cross-flow are not strong enough. At increasing z distances, when the stresses imposed by the cross-flow reaches sufficiently high levels, the flow initiates and generates a variation of shear rate and shear stress within the concentration polarization layer, area B.

These results highlight that the levels of stresses which define the initiation of the flow at the interface of areas A and B, will adapt to the filtered system according to the level of concentration involved to permit a flow at a certain level of stress.

CONCLUSION

This work has developed *in-situ* SAXS, *in-situ* micro-PIV during cross-flow ultrafiltration process of CNC suspensions. Combined with rheological measurements and the corresponding rheological laws of these suspensions, the calculation of the shear stress inside the accumulated layers has been accessible for the first time in these kinds of colloidal suspensions. A better understanding of the structural and kinematic evolutions of the concentrated layers has been established and linked to the rheological behavior evolution of the suspensions as a function of volume fraction and filtration conditions. The results of SAXS experiments performed *in-situ* during the filtration process have allowed highlighting increase of the volume fraction as a function of the distance z above the membrane surface during the filtration time. The anisotropy increase of the 2D-SAXS patterns at increasing filtration times and decreasing distances from the membrane surface, has allowed linking the concentration phenomena to a specific regular orientation of the nanocrystals inside the accumulated layers during the filtration. For the first time, velocity fields within the accumulated layers were measured for CNC's suspensions for a

hundred microns above the membrane surface. Rheometric measurements of unsonicated CNC's suspensions were performed in wide range of concentrations, for level of concentration which can be reached in the concentrated layers. The *in-situ* stress field of the concentrated layers has then been calculated by the integration of the rheological laws into the *in-situ* shear rate fields obtained from the velocity field by micro-PIV. The correlation of these original results bring us the knowledge on the existence of 3 different behavior regions within the filtration channel, depending on the volume fraction, the shear rate and the shear stress values. The first region A corresponding to the fouling layer behavior has been emphasized. The level of volume fraction reaches in this area, corresponding to a shear thinning behavior, is high enough to resist to the flow induces by the cross-flow in this layer. A second region B occurs when the volume fraction reaches a low value (below 3 vol%) further from the membrane surface. The local shear-flow forces are high enough to allow the particles accumulated starting to flow. This highlights the transition from the fouling to the polarization concentration layer. This area transition from region A to B is associated to a transition from shear-thinning fluid to Newtonian fluid behavior of the CNC suspensions. Then in the last region C, the shear rate decreases with the corresponding shear stress until reaching the conditions where the suspension is circulating in the feed channel without being influenced by the accumulated particles. From a fundamental point of view, the knowledge of the shear stress levels linked to the rheological behavior of the fluid of interest allows a better understanding of the phenomena involved in the formation of the concentrated layers. From an industrial point of view, it permits preventing from these phenomena occurring during high scale processes. This study allows quantifying the important influencing parameters of the filtration performance in order to reach an increasing yield of CNC production at an industrial scale.

AUTHOR INFORMATION

Corresponding Authors

*E-mail: frederic.pignon@univ-grenoble-alpes.fr

*E-mail: nicolas.hengl@univ-grenoble-alpes.fr

Author Contributions

The manuscript was written through contributions of all authors. All authors have given approval to the final version of the manuscript.

Notes

The authors declare no competing financial interest

ACKNOWLEDGMENTS

We would like to thank Theyencheri Narayanan and Michael Sztucki (ESRF, Grenoble) for fruitful discussions and for their kind help in scattering experiments, Jean-Jacques Lasserre (Dantec Dynamics) for productive discussions and for his help in the micro-PIV Measurements.

We thank Eric Faivre, H el ene Galliard, Didier Bl es es and Fr ed eric Hugenell (Laboratoire Rh eologie et Proc ed es, Grenoble) and Jacques Gorini (ESRF, Grenoble) for technical assistance.

We gratefully acknowledge the ESRF for the SC 4177 beam time allocation. This work was supported by the Labex TEC 21 (Investissements d'Avenir - grant agreement n o ANR-11-LABX-0030). LRP and LGP2 are part of PolyNat Carnot Institut (Investissements d'Avenir - grant agreement no. ANR-11-CARN-030-01) and of program (ANR-15-IDEX-02).

REFERENCES

- (1) Siqueira, G.; Bras, J.; Dufresne, A. Cellulosic Bionanocomposites: A Review of Preparation, Properties and Applications. *Polymers* **2010**, *2*, 728-765.

- (2) Kalia, S.; Dufresne, A.; Cherian, B.M.; Kaith, B.S.; Avérous, L.; Niuguna, J.; Nassiopoulo, E. Cellulose-based Bio- and Nanocomposites: A Review. *Int. J. Polym. Sci.* **2011**, *2011*, 837875.
- (3) . Bardet, R.; Belgacem, N.; Bras, J. Flexibility and Color Monitoring of Cellulose Nanocrystal Iridescent Solid Films Using Anionic or Neutral Polymers. *ACS Appl. Mater. Interfaces* **2015**, *7*, 4010-4018.
- (4) Dufresne, A. *Nanocellulose: From Nature to High Performance Tailored materials*, 2nd ed.; Walter de Gruyter GmbH, Berlin/Boston, 2017.
- (5) Kargarzadeh, H.; Huang, J.; Lin, N.; Ahmad, I.; Mariano, M.; Dufresne, A.; Thomas, S.; Gałęski, A. Recent Developments in Nanocellulose-based Biodegradable Polymers, Thermoplastic Polymers, and Porous Nanocomposites. *Prog. Polym. Sci.* **2018**, *87*, 197-227.
- (6) Romero, C.A.; Davis, R.H. Global Model of Crossflow Microfiltration Based on Hydrodynamic Particle Diffusion. *J. Membr. Sci.* **1988**, *39*, 157-185.
- (7) Song, L.; Elimelech, M. Theory of Concentration Polarization in Crossflow Filtration. *J. Chem. Soc., Faraday Trans.* **1995**, *91*, 3389-3398.
- (8) Bowen, W.R.; Williams, P.M. Quantitative Predictive Modelling of Ultrafiltration Processes: Colloidal Science Approaches. *Adv Colloid Interface Sci.* **2007**, *134-135*, 3-14.
- (9) Elimelech, M.; Bhattacharjee, S. A Novel Approach for Modeling Concentration Polarization in Crossflow Membrane Filtration Based on the Equivalence of Osmotic Pressure Model and Filtration Theory. *J. Membr. Sci.* **1998**, *145*, 223-241.
- (10) Bacchin, P.; Si-Hassen, D.; Starov, V.M.; Clifton, J.; Aimar, P. A Unifying Model for Concentration Polarization, Gel-layer Formation and Particle Deposition in Cross-flow Membrane Filtration of Colloidal Suspensions. *Chem. Eng. Sci.* **2002**, *57*, 77-91.

- (11) Bacchin, P.; Aimar, P.; Sanchez, V. Model for Colloidal Fouling of Membranes. *AIChE J.* **1995**, *41*, 368-376.
- (12) Chen, V.; Li, H.; Fane, A.G. Non-invasive Observation of Synthetic Membrane Processes - A Review of Methods. *J. Membr. Sci.* **2004**, *241*, 23-44.
- (13) Marselina, Lifa, Y.; Le-Clech, P.; Stuetz, R.M.; Chen, V. Characterisation of Membrane Fouling Deposition and Removal by Direct Observation Technique. *J. Membr. Sci.* **2009**, *341*, 163-171.
- (14) Huang, X.; Guillen, G.R.; Hoek, E.M.V. A New High-pressure Optical Membrane Module for Direct Observation of Seawater RO Membrane Fouling and Cleaning. *J. Membr. Sci.* **2010**, *364*, 149-156.
- (15) Beaufort, S.; Alfenore, S.; Lafforgue, C. Use of Fluorescent Microorganisms to Perform in vivo and in situ Local Characterization of Microbial Deposits. *J. Membr. Sci.* **2011**, *369*, 30-39.
- (16) Fernandez-Sempere, J.; Ruiz-Bevia, F.; Salcedo-Diaz, R. Measurements by Holographic Interferometry of Concentration Profiles in Dead-end Ultrafiltration of Polyethylene Glycol Solutions. *J. Membr. Sci.* **2004**, *229*, 187-197.
- (17) Airey, D.; Yao, S.; Wu, J.; Chen, V.; Fane, A.G.; Pope, J.M. An Investigation of Concentration Polarization Phenomena in Membrane Filtration of Colloidal Silica Suspensions by NMR Micro. *J. Membr. Sci.* **1998**, *145*, 145-158.
- (18) Mendret, J.; Guigui, C.; Schmitz, P.; Cabassud, C.; Duru, P. An Optical Method for in situ Characterization of Fouling during Filtration. *AIChE J.* **2007**, *53*, 2265-2274.

- (19) Mendret, J.; Guigui, C.; Cabassud, C.; Schmitz, P. Dead-end Ultrafiltration and Backwash: Dynamic Characterisation of Cake Properties at Local Scale.*Desalination***2006**,*199*, 216-218.
- (20) Mendret, J.; Guigui, C.; Schmitz, P.; Cabassud, C. In situ Dynamic Characterisation of Fouling under Different Pressure Conditions during Dead-end Filtration: Compressibility Properties of Particle Cakes.*J. Membr. Sci.***2009**,*333*, 20-29.
- (21) Agbangla, G.C.; Climent, É.; Bacchin, P. Experimental Investigation of Pore Clogging by Microparticles: Evidence for a Critical Flux Density of Particle Yielding Arches and Deposits.*Sep. Purif. Technol.***2012**,*101*, 42-48.
- (22) Sendekie, Z.B.; Bacchin, P. Colloidal Jamming Dynamics in Microchannel Bottlenecks.*Langmuir***2016**,*32*, 1478-1488.
- (23) Lorenzen, S.; Ye, Y.; Chen, V.; Christensen, M.L. Direct Observation of Fouling Phenomena during Cross-flow Filtration: Influence of Particle Surface Charge.*J. Membr. Sci.***2016**,*510*, 546-558.
- (24) Mattsson, T.; Lewis, W.J.T.; Chew, Y.M.J.; Bird, M.R. The Use of Fluid Dynamic Gauging in Investigating the Thickness and Cohesive Strength of Cake Fouling Layers Formed during Cross-flow Microfiltration.*Sep. Purif. Technol.***2018**,*198*, 25-30.
- (25) Su, T.J.; Lu, J.R.; Cui, Z.F.; Thomas, R.K.; Heenan, R.K. Application of Small Angle Neutron Scattering to the in situ Study of Protein Fouling on Ceramic Membranes.*Langmuir***1998**,*14*, 5517-5520.
- (26) Antelmi, D.; Cabane, B.; Meireles, M.; Aimar, P. Cake Collapse in Pressure Filtration.*Langmuir***2001**,*17*, 7137-7144.

- (27) Madeline, J.B.; Meireles, M.; Bourgerette, C.; Botet, R.; Schweins, R.; Cabane, B. Restructuring of Colloidal Cakes during Dewatering. *Langmuir* **2007**, *23*, 1645-1658.
- (28) Pignon, F.; Magnin, A.; Piau, J.-M.; Cabane, B.; Aimar, P.; Meireles, M.; Lindner, P. Structural Characterisation of Deposits Formed during Frontal Filtration. *J MembrSci*, 2000, *174*, 189-204.
- (29) Pignon, F.; Alemdar, A.; Magnin, A.; Narayanan, T. Small-Angle X-ray Scattering Studies of Fe-Montmorillonite Deposits during Ultrafiltration in a Magnetic Field. *Langmuir* **2003**, *19*, 8638-8645.
- (30) Pignon, F.; Belina, G.; Narayanan, T.; Paubel, X.; Magnin, A.; Gésan-Guiziou, G. Structure and Rheological Behavior of Casein Micelle Suspensions during Ultrafiltration Process. *J. Chem. Phys.* **2004**, *21*, 8138-8146.
- (31) David, C.; Pignon, F.; Narayanan, T.; Sztucki, M.; Gesan-Guiziou, G.; Magnin, A. Spatial and Temporal in situ Evolution of the Concentration Profile during Casein Micelle Ultrafiltration Probed by Small-angle X-ray Scattering. *Langmuir* **2008**, *24*, 4523-4529.
- (32) Rey, C.; Hengl, N.; Baup, S.; Karrouch, M.; Dufresne, A.; Djeridi, H.; Dattani, R.; Pignon, F. Velocity, Stress and Concentration Fields Revealed by Micro-PIV and SAXS Within Concentration Polarization Layers during Cross-flow Ultrafiltration of Colloidal Laponite Clay Suspensions. *J. Membr. Sci.* **2019**, *578*, 69-84.
- (33) Pignon, F.; Abyan, M.; David, C.; Magnin, A.; Sztucki, M. In Situ Characterization by SAXS of Concentration Polarization Layers during Cross-Flow Ultrafiltration of Laponite Dispersions. *Langmuir* **2012**, *28*, 1083-1094.
- (34) Jin, Y.; Hengl, N.; Baup, S.; Pignon, F.; Gondrexon, N.; Magnin, A.; Sztucki, M.; Narayanan, T.; Michot, L.; Cabane, B. Effects of Ultrasound on Colloidal Organization at

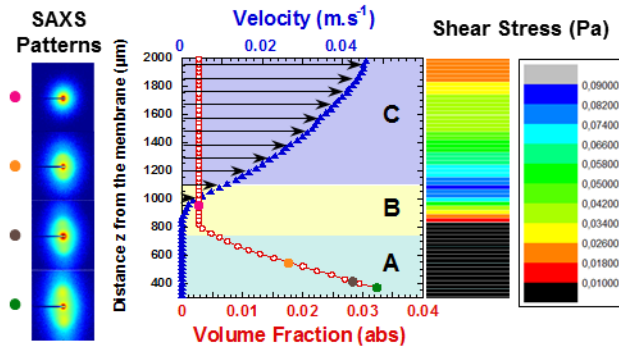
Nanometer Length Scale during Cross-flow Ultrafiltration Probed by in-situ SAXS.*J.*

Membr. Sci. **2014**,*453*, 624-635.

- (35) Jin Y.; Hengl N.; Baup S.; Pignon F.; Gondrexon N.; Sztucki M.; Romdhane, A.; Guillet A.; Aurousseau M. Ultrasonic assisted cross-flow ultrafiltration of starch and cellulose nanocrystals suspensions: Characterization at multi-scales. *Carbohydrate Polymers*, **2015**, *124*, 66-76.
- (36) Jin, Y.; Hengl, N.; Baup, S.; Maitrejean, G.; Pignon, F. Modeling and Analysis of Concentration Profiles Obtained by in-situ SAXS during Cross-flow Ultrafiltration of Colloids.*J.Membr.Sci*,**2017**,*528*, 34-45.
- (37) Cano, G.; Steinle, P.; Daurelle, J.-V.; Wyart, Y.; Glucina, K.; Bourdiol, D.; Moulin, P. Determination of Pressure and Velocity Fields in Ultrafiltration Membrane Modules Used in Drinking Water Production.*J. Membr. Sci.* **2013**,*431*, 221-232.
- (38) Kim, H.T.; Cha, J.E.; Rhee, B.W.; Choi, H.-L.; Seo, H.; Bang, I.C. *Measurement of Velocity and Temperature Profiles in the Scaled-down Candu-6 Moderator Tank*. New York: Amer. Soc. Mechanical Engineers, **2014**.
- (39) Arndt, F.; Roth, U.; Nirschl, H.; Schütz, S.; Guthausen, G. New Insights into Sodium Alginate Fouling of Ceramic Hollow Fiber Membranes by NMR Imaging. *AIChE J.* **2016**,*62*, 2459-2467.
- (40) Gicquel, E.; Bras, J.; Rey, C.; Putaux, J.-L.; Pignon, F.; Martin, C. Impact of Sonication on the Rheological and Colloidal Properties of Highly Concentrated Cellulose Nanocrystal Suspensions. *Cellulose* **2019**, under revision.

- (41) Narayanan, T.; Sztucki, M.; Vaerenbergh, P. V.; Léonardon, J.; Gorini, J.; Claustre, L.; Sever, F.; Morse, J.; Boesecke, P. A multipurpose instrument for time-resolved ultra-small-angle and coherent X-ray scattering. *J. Appl. Cryst.* **2018**, *51*, 1511-1524.
- (42) Urena-Benavides, E.E.; Ao, G.; Davis, V.A.; Kitchens, C.L. Rheology and Phase Behavior of Lyotropic Cellulose Nanocrystal Suspensions. *Macromolecules* **2011**, *44*, 8990-8998.
- (43) Shafiei-Sabet, S.; Hamad, W.Y.; Hatzikiriakos, S.G. Rheology of Nanocrystalline Cellulose Aqueous Suspensions. *Langmuir* **2012**, *28*, 17124-17133.
- (44) Schutz, C.; Agthe, M.; Fall, A.B.; Gordeyeva, K.; Guccini, V.; Salajková, M.; Plivelic, T.S.; Lagerwall, J.P.F.; Salazar-Alvarez, G.; Bergström, L. Rod Packing in Chiral Nematic Cellulose Nanocrystal Dispersions Studied by Small-Angle X-ray Scattering and Laser Diffraction. *Langmuir* **2015**, *31*, 6507-6513.
- (45) Aimar, P.; Bacchin, P. Slow Colloidal Aggregation and Membrane Fouling. *J. Membr. Sci.*, 2010, *360*, 70-76.
- (46) Trappe, V.; Prasad, V.; Cipelletti, L.; Segre, P.N.; Weitz, D.A. Jamming Phase Diagram for Attractive Particles. *Nature* **2001**, *411*, 772-775.

For Table of Contents Use Only



Understanding of concentration phenomena governing the ultrafiltration performances in order to reach an increasing yield of nanocrystal celluloses production at industrial scale.